

RESEARCH

Open Access



In vitro oxidative decarboxylation of free fatty acids to terminal alkenes by two new P450 peroxygenases

Huifang Xu^{1,2}, Linlin Ning^{1,2,4}, Wenxia Yang^{1,2}, Bo Fang^{1,2}, Cong Wang^{1,2}, Yun Wang^{2,3}, Jian Xu^{2,3}, Severine Collin⁵, Frederic Laeuffer⁵, Laurent Fourage⁵ and Shengying Li^{1,2*}

Abstract

Background: P450 fatty acid decarboxylases represented by the unusual CYP152 peroxygenase family member OleT_{JE} have been receiving great attention recently since these P450 enzymes are able to catalyze the simple and direct production of 1-alkenes for potential applications in biofuels and biomaterials. To gain more mechanistic insights, broader substrate spectra, and improved decarboxylative activities, it is demanded to discover and investigate more P450 fatty acid decarboxylases.

Results: Here, we describe for the first time the expression, purification, and in vitro biochemical characterization of two new CYP152 peroxygenases, CYP-Aa162 and CYP-Sm46Δ29, that are capable of decarboxylating straight-chain saturated fatty acids. Both enzymes were found to catalyze the decarboxylation and hydroxylation of a broad range of free fatty acids (C₁₀–C₂₀) with overlapping substrate specificity, yet distinct chemoselectivity. CYP-Sm46Δ29 works primarily as a fatty (lauric) acid decarboxylase (66.1 ± 3.9% 1-undecene production) while CYP-Aa162 more as a fatty (lauric) acid hydroxylase (72.2 ± 0.9% hydroxy lauric acid production). Notably, the optical spectroscopic analysis of functional CYP-Sm46Δ29 revealed no characteristic P450 band, suggesting a unique heme coordination environment. Active-site mutagenesis analysis showed that substitution with the proposed key decarboxylation-modulating residues, His85 and Ile170, enhanced the decarboxylation activity of CYP-Aa162 and P450_{B5β}, emphasizing the importance of these residues in directing the decarboxylation pathway. Furthermore, the steady-state kinetic analysis of CYP-Aa162 and CYP-Sm46Δ29 revealed both cooperative and substrate inhibition behaviors which are substrate carbon chain length dependent.

Conclusions: Our data identify CYP-Sm46Δ29 as an efficient OleT_{JE}-like fatty acid decarboxylase. Oxidative decarboxylation chemoselectivity of the CYP152 decarboxylases is largely dependent upon the carbon chain length of fatty acid substrates and their precise positioning in the enzyme active site. Finally, the kinetic mode analysis of the enzymes could provide important guidance for future process design.

Keywords: Alkenes, Biofuels, P450 fatty acid decarboxylases, Substrate specificity, Chemoselectivity, Site-directed mutagenesis, Enzyme kinetics

Background

Cytochrome P450 (CYP) enzymes are a superfamily of important biocatalysts that perform an extraordinary

breadth of biochemical reactions [1–3], and have been widely applied to oxidation of complex organic substrates and biosynthesis of chemical building block molecules [4–6]. Among diverse P450 products, terminal alkenes (i.e., α-alkenes or 1-alkenes) have significant industrial potential and outstanding economic importance, given that these hydrocarbons highly mimic the chemical composition and physical properties of fossil fuels

*Correspondence: lishengying@qibebt.ac.cn

¹ Shandong Provincial Key Laboratory of Synthetic Biology, Qingdao Institute of Bioenergy and Bioprocess Technology, Chinese Academy of Sciences, No. 189 Songling Road, Qingdao 266101, Shandong, China
Full list of author information is available at the end of the article

[7–10]. There has been widespread biotechnological interest focusing on the identification and reconstitution of enzymes and pathways capable of synthesizing biohydrocarbons in microbial hosts [7, 9, 11–17]. A sustainable biosynthetic route to 1-alkenes from biologically abundant feedstocks such as free fatty acids (FFAs) clearly represents a promising pathway. In 2011, Rude et al. [13] reported the first one-step enzymatic oxidative decarboxylation of FFAs by a P450 peroxygenase OleT_{JE}, isolated from *Jeotgalicoccus* sp. ATCC 8456, to yield long-chain (C₁₃–C₁₉) 1-alkenes.

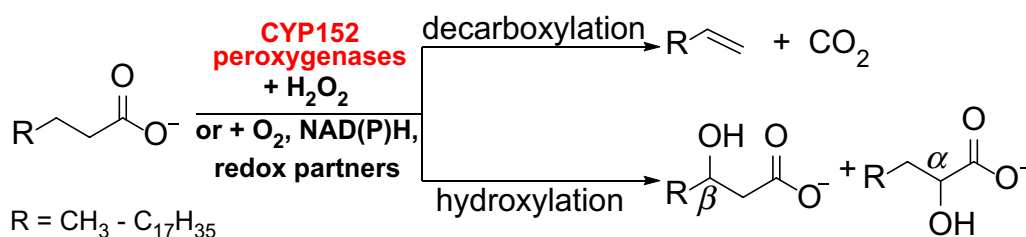
In view of its tremendous potential for biological production of terminal olefins, OleT_{JE} since its discovery has captured great attention within academia and industry. A fast growing number of studies have been carried out to optimize OleT_{JE} catalysis and to understand its catalytic mechanism [16, 18–28]. These include the development of alternative catalytic systems (e.g., the O₂/NAD(P)H/redox partners system [16] and the light-driven H₂O₂ generation system [21]) (Scheme 1), the determination of OleT_{JE} crystal structures [18, 28], the elucidation of catalytically reactive species [19, 20], and the expansion of substrate scope to structurally different aromatic carboxylic acids [29], dionic acids (to produce dienes) [30], and even some unnatural substrates including styrene, nonane, and cyclohexane [31].

Mechanistically, a majority of P450s use O₂ and NAD(P)H-dependent redox systems to catalyze diverse oxidative/monooxygenation reactions [32, 33]. However, there are a small number of P450s that evolved to naturally utilize H₂O₂ as the sole oxygen and electron donor to catalyze oxidative reactions through the so-called peroxide shunt pathway [33–35]. These enzymes are referred to as P450 peroxygenases. The best-characterized P450 peroxygenases are among the CYP152 [36] family members, including P450_{BSβ} (CYP152A1) from *Bacillus subtilis* [35] and P450_{SPα} (CYP152B1) from *Sphingomonas paucimobilis* [34]. OleT_{JE}, based on its amino acid sequence similarity, was designated as CYP152L1 [13, 18]. Within the CYP152 members that have been biochemically characterized so far, P450_{SPα}

catalyzes exclusively the Cα hydroxylation of FFAs [34], and P450_{BSβ} generates both α- and β-hydroxy fatty acids as major products but with a small amount of 1-alkene as well [13, 35, 37]. A recently characterized CYP-MP peroxygenase [24] is able to introduce the hydroxyl group at α-, β-, γ-, δ-, and ε-positions of C₁₂–C₁₈ fatty acids, but it only displayed marginal decarboxylation activity against myristic acid (C₁₄) and palmitic acid (C₁₆). Heretofore, OleT_{JE} is the only one to predominantly catalyze the decarboxylation of long-chain fatty acids generating 1-alkenes as the major products and α- and β-hydroxy fatty acids as the side products (Scheme 1) [13, 16, 22]. It would be of great interest and importance to explore more P450 fatty acid decarboxylases and expand the enzyme inventory for future broader biotechnological applications.

In an attempt to screen for biocatalysts capable of converting medium-chain C₁₂ fatty acid (lauric acid) to 1-undecene for potential applications in biofuels and biolubricants, two new P450 sequences, CYP-Aa162 (CYP152A8, GenBank Accession Number: WP_008340313) from *Alicyclobacillus acidocaldarius* LAA1 and CYP-Sm46 (CYP152L2, GenBank Accession Number: EKV50422) from *Staphylococcus massiliensis* S46, were identified apart from OleT_{JE} and P450_{BSβ}. To better harness these two uncharacterized CYP152 family members for future industrial applications, and to further our understanding of the unique decarboxylation mechanism employed by CYP152 decarboxylases, we sought to characterize the detailed biochemical properties of the two enzymes.

In this study, we cloned, expressed, and purified CYP-Aa162 and CYP-Sm46 enzymes and in vitro characterized their catalytic activities towards a panel of different carbon chain length fatty acid substrates. Analytical data demonstrated that CYP-Aa162 acts mainly as a P450_{BSβ}-like fatty acid hydroxylase, whereas CYP-Sm46 acts as an efficient OleT_{JE}-like fatty acid decarboxylase. Their substrate conversion rates and regio- and chemoselectivity exhibited significant substrate carbon chain length dependence. In addition, our enzymatic kinetic



Scheme 1 Fatty acid decarboxylation and hydroxylation catalyzed by CYP152 peroxygenases

analysis suggested that the metabolism of fatty acids by the CYP152 enzymes could undergo both cooperative and substrate inhibition behaviors, providing important information and guidance for future process design.

Results

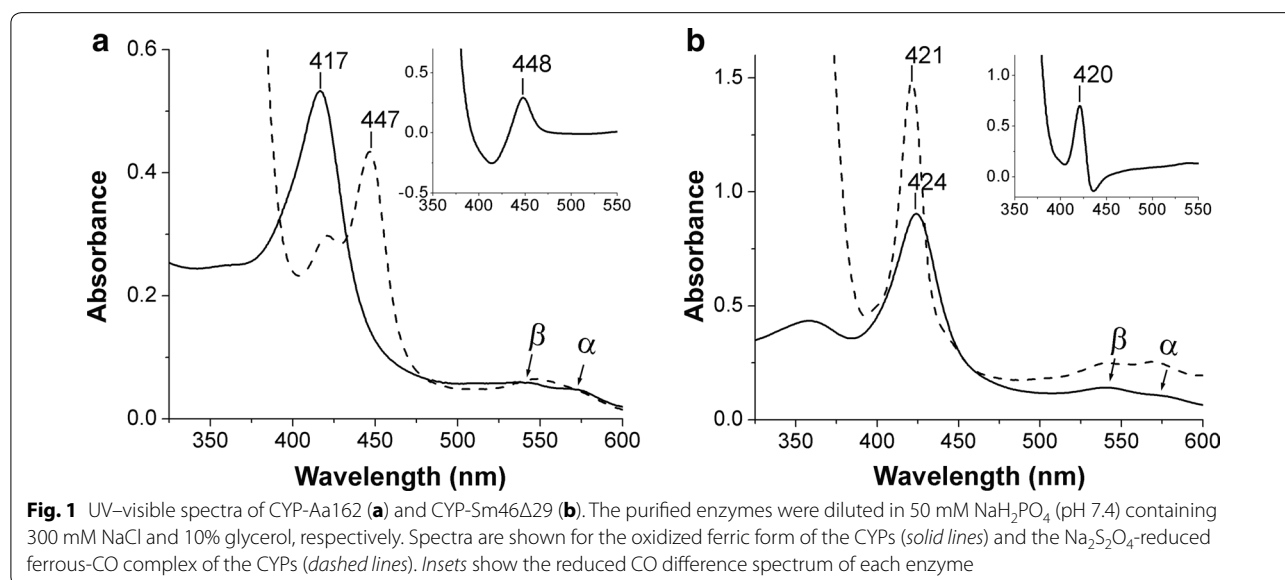
Heterologous expression and purification of CYP-Aa162 and CYP-Sm46 Δ 29

According to protein sequence alignment (Additional file 1: Figure S1), CYP-Aa162 has 64% (39%) sequence identity to P450_{B β} (OleT_{JE}), while CYP-Sm46 is 65% (37%) identical to OleT_{JE} (P450_{B β}). Heterologous expression of CYP-Aa162 in *E. coli* (with its encoding sequence codon-optimized) led to an appreciable level of the recombinant protein purified to near homogeneity (Additional file 1: Figure S2). However, for CYP-Sm46, the original construct of pET28b-CYP-Sm46 (codon-optimized) showed very poor expression and solubility, which did not improve upon subcloning into an alternative expression vector pCWori [38] or by optimization of the expression conditions. This prompted us to re-examine the protein sequence of EKV50422 and its annotation. We found that this sequence has an extra long (~29 amino acids) *N* terminus with no functional annotations when compared with most other CYP152 members including those cytochrome P450 family proteins from other *Staphylococcus* species (Additional file 1: Figure S1). Analyses of the CYP-Sm46 protein sequence using several protein prediction tools such as Phobius, TMHMM 2.0, and SignalP 4.1 [39–41] also showed no positive return of either a signal peptide or transmembrane helices within the *N*-terminal region of 60 amino acids. A further BLAST search revealed a recently added

(17-Jan-2015) ‘truncated’ entry of CYP-Sm46 (GenBank Accession Number: WP_039990689), hereafter called CYP-Sm46 Δ 29, which decodes from an alternative start codon (GUG) and therefore has the 29 *N*-terminal amino acids removed. Subsequent expression of this shorter version CYP-Sm46 Δ 29 led to significantly improved protein production and solubility, and the protein was then purified to near homogeneity (Additional file 1: Figure S2). The codon-optimized gene sequences of CYP-Aa162 and CYP-Sm46 Δ 29, and their corresponding amino acid sequences are shown in Additional file 2.

UV-visible spectroscopic properties of CYP-Aa162 and CYP-Sm46 Δ 29

The resting ferric form of CYP-Aa162 (Fig. 1a) exhibited a typical low-spin (LS) water-bound P450 heme spectrum with its Soret absorption peak at 417 nm and the smaller α - and β -bands in the visible region at ~566 and ~538 nm, respectively. These values are similar to those of OleT_{JE} (418, 535, 566 nm) [18] and other LS bacterial P450s (e.g., the heme domain of CYP102A1 (P450_{B β M3}) from *Bacillus megaterium* with maxima at 418, 534, and 568 nm) [42]. However, CYP-Aa162 displayed no obvious hyperporphyrin (split Soret) characteristic at ~360 nm, which is different from that of OleT_{JE} [18]. A widely accepted criterion for the identification of cytochrome P450 is a Soret peak at around 450 nm in the reduced CO difference spectrum. Here, for CYP-Aa162, both the reduced CO difference spectrum and the absolute absorption spectrum of the dithionite-reduced Fe²⁺-CO adducts featured a characteristic thiolate-ligated P450 Soret band at 447–448 nm (Fig. 1a and inset), which is similar to that of P450_{B β} with a peak at 446 nm [35].



However, the purified ferric form of CYP-Sm46 Δ 29 displayed a red-shifted Soret band at 422–424 nm, followed by a small but prominent β band at 540 nm and a significantly weaker and flat α band at 571 nm (Fig. 1b). Prominent hyperporphyrin characteristics (split Soret) are visible at 360 nm. These features are similar to those reported for CYP-MP (maxima at 422, 545, and 575 nm) [24], but different from the typical 418, ~535, and ~568 nm maxima for LS water-bound P450s [18, 42]. These altered spectroscopic features may indicate an imidazole-coordinated or more likely a distal hydroxyl-coordinated ferric LS heme form as suggested in the CYP-MP [24]. Furthermore, much to our surprise, reduction of the CYP-Sm46 Δ 29 with sodium dithionite in the presence of CO revealed no characteristic P450 peak at ~450 nm. The maximum absorption of this Fe²⁺-CO adduct was still at ~421 nm with enhanced α - and β -bands. Correspondingly, the reduced CO difference spectrum of CYP-Sm46 Δ 29 also exhibited only the P420 peak (Fig. 1b inset). Attempts to produce a detectable P450 species by altering the amount of dithionite, buffer pH, and by substrate-aided stabilization of any, if exists, P450-CO adduct as the case with P450 EpoK enzyme [43] all proved negative (Additional file 1: Figure S3). The similar ‘P420’ spectra were observed in all preparations of the enzyme unanimously. These data suggest that CYP-Sm46 Δ 29 is somehow incapable of forming a detectable cysteine thiolate-ligated Fe²⁺-CO adduct. We speculate that this unusual spectroscopic feature may arise either from simple protonation of the proximal cysteine thiolate to a neutral thiol form [43, 44], or from dissociation of the thiolate ligand from the heme iron, followed

by coordination of an alternative proximal ligand such as a histidine in the case with the pressure-induced P420_{cam} [45, 46], or from other reduction-linked structural alterations that prevent the formation of thiolate-ligated ferrous-CO species. Nevertheless, these altered spectroscopic features did not affect the enzyme’s peroxygenase activity as shown below.

Inability of CYP-Aa162 and CYP-Sm46 Δ 29 to elicit monooxygenase activity

To check if a class I electron transfer system could afford a P450 Soret feature in CYP-Aa162 and CYP-Sm46 Δ 29 [47], we examined the UV–visible spectra of the two enzymes in an NAD(P)H/redox proteins/CO system. As a result, while the control P450 monooxygenase P450_{BM3} was successfully reduced by the addition of NADP_{BM3} and exhibited an almost complete transition to P450 spectrum in the presence of lauric acid (LA) substrate (Additional file 1: Figure S4), neither CYP-Aa162 nor CYP-Sm46 Δ 29 showed a P450 chromophore after incubation with the redox partner proteins CamAB (i.e., putidaredoxin reductase and putidaredoxin that are able to support the in vitro activity of both P450 enzymes, see below) and their optimal cofactor NADH in the presence of LA (Fig. 2a). Further catalytic activity assay indicated that the two enzymes exhibited appreciable LA conversion activity in the H₂O₂ system. However, their activity was dramatically diminished in the O₂/CamAB/NADH reaction system when high concentrations of catalase were added to remove H₂O₂ potentially generated from the decoupling of NADH oxidation (Fig. 2b), implying that CYP-Aa162 and CYP-Sm46 Δ 29 have very little or

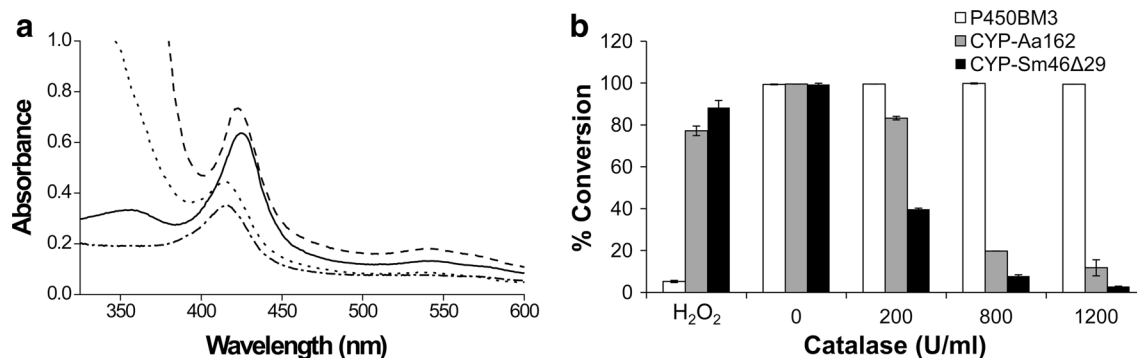


Fig. 2 UV–visible spectra and lauric acid (LA) conversion activity of CYP-Aa162 and CYP-Sm46 Δ 29 in the O₂/redox partners/NAD(P)H system. **a** The UV–visible spectra are, respectively, shown for the substrate LA-bound ferric form of CYP-Sm46 Δ 29 with a Soret band at 422 nm (solid line); the CamAB/NADH ‘reduced’ CO-bound form of CYP-Sm46 Δ 29 with the Soret peak still at ~422 nm (dashed line); the substrate LA-bound ferric form of CYP-Aa162 with a Soret band at ~418 nm (dashed and dotted line); the CamAB/NADH ‘reduced’ CO-bound form of CYP-Aa162 with an unshifted Soret peak (dotted line). **b** Enzymatic conversion of lauric acid by CYP-Aa162, CYP-Sm46 Δ 29, and the control P450_{BM3} monooxygenase in the O₂/redox proteins/NAD(P)H system in the absence or presence of different concentrations of catalase. For CYP-Aa162 and CYP-Sm46 Δ 29, CamAB/NADH was used for the electron transfer cascade. For the self-sufficient P450_{BM3} enzyme, NADPH was used as the electron donor. Conversions of the substrate in the H₂O₂ cofactor system were included as controls

no monooxygenase activity. The marginal residual activity of the two enzymes shown at 1200 U mL^{-1} catalase condition may represent some inevitable leakage of H_2O_2 to the P450 proteins, as even in the absence of putidaredoxin there was still meager activity detectable at this high catalase concentration (Additional file 1: Figure S5).

Substrate specificity and chemoselectivity of CYP-Aa162 and CYP-Sm46Δ29

Members in the CYP152 peroxygenase family are capable of utilizing H_2O_2 as the sole electron and oxygen donor to carry out catalytic reactions [33]. Among those CYP152s that have been biochemically characterized so far, OleT_{JE} catalyzes predominantly the decarboxylation of long-chain fatty acids to give 1-alkenes as the main products and α - and β -hydroxy fatty acids as the side products [13]. Other CYP152 enzymes including P450_{SP α} , P450_{BS β} , and CYP-MP catalyze primarily the hydroxylation of free fatty acids, introducing the hydroxyl group at varying carbon positions (i.e., α -, β -, γ -, δ -, or ϵ -position) [24, 34, 35, 37]. Here, in order to investigate the substrate specificity and chemoselectivity (decarboxylation vs hydroxylation) of the two new CYP152 enzymes, we set out to examine their catalytic reactions towards a range of different carbon chain length (C_{10} – C_{20}) FFAs using H_2O_2 as the sole cofactor.

As a result, both enzymes exhibited quite similar substrate preference profiles with lauric acid (C_{12}) being the best substrate (Fig. 3). Its conversion ratios were 77.3 ± 1.0 and $83.5 \pm 3.4\%$ by CYP-Aa162 and CYP-Sm46Δ29, respectively. In addition, CYP-Sm46Δ29 also converted myristic acid (C_{14}) efficiently ($74.5 \pm 3.5\%$). However, in terms of decarboxylation, CYP-Aa162 showed only marginal alkene production from its best substrate C_{12} ($5.1 \pm 0.1\%$), whereas CYP-Sm46Δ29 exhibited significantly higher percentage of alkene production.

The optimal substrates C_{12} and C_{14} FFAs reached the alkene production efficiency of 66.1 ± 3.9 and $57.4 \pm 3.6\%$, respectively. Unlike previously reported for OleT_{JE} by others [13, 21], CYP-Sm46Δ29 favors more the medium-chain length fatty acids (C_{12} or C_{14}) rather than the long ones (C_{16} – C_{20}). The decarboxylation activity of CYP-Sm46Δ29 (Fig. 3) and the ratio of decarboxylation over hydroxylation activities (Additional file 1: Figure S6) gradually reduced after C_{12} with the increase in substrate carbon chain length, and the hydroxyl FAs became the major products in the reactions with C_{18} or C_{20} as a substrate, indicating that different substrate binding modes are likely employed by this enzyme.

In consideration of the high sequence identity (64%) and similar UV–visible absorption maxima between CYP-Aa162 and P450_{BS β} , we compared their catalytic activities in parallel. As shown in Fig. 4, the two enzymes exhibited very similar substrate preference spectra and total fatty acid conversion efficiency. However, P450_{BS β} showed generally higher alkene production ratios compared with CYP-Aa162. The best alkene-producing substrate lauric acid (C_{12}) displayed a fivefold higher 1-undecene production ($27.7 \pm 0.9\%$ versus $5.1 \pm 0.1\%$). Nonetheless, substrate hydroxylation still represented the major chemistry of the two enzymes, which is not surprising since P450_{BS β} was initially identified as a P450 fatty acid hydroxylase [35]. The hydroxylation versus decarboxylation ratios of the two CYPs towards their preferred C_{10} – C_{14} substrates were at least 2.5:1. Thus, we designated CYP-Aa162 as a P450_{BS β} -like fatty acid hydroxylase rather than a P450 decarboxylase.

Furthermore, to comparatively investigate the detailed product distribution, the C_{14} substrate myristic acid was reacted with the four enzymes CYP-Aa162, CYP-Sm46Δ29, P450_{BS β} , and OleT_{JE}, respectively. The results (Table 1) revealed that CYP-Aa162 formed

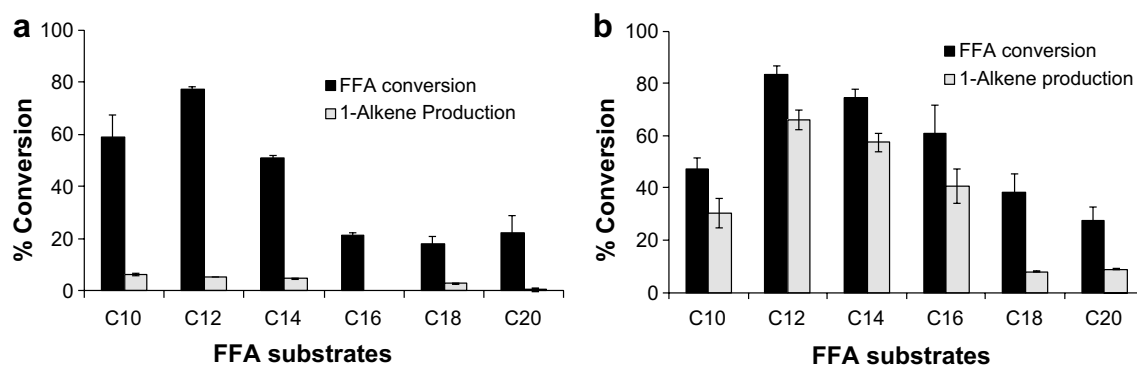


Fig. 3 Substrate preference and 1-alkene production profiles of CYP-Aa162 (a) and CYP-Sm46Δ29 (b). Substrate preference was determined by calculating the percentage conversion of each fatty acid substrate. The corresponding 1-alkene production represents the percentage of 1-alkene yield over the starting substrate. Results shown are mean \pm SD of duplicated experiments

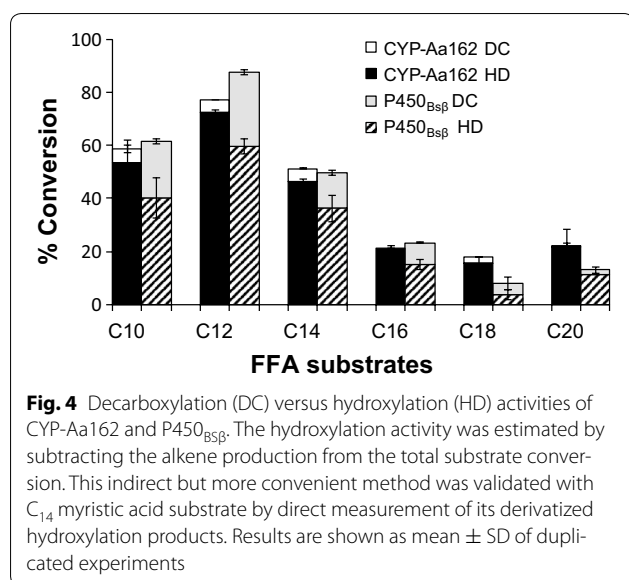


Table 1 GC-MS analysis of catalytic activities and product distribution profiles of the selected CYP152 peroxxygenases towards myristic acid (C₁₄)

| Enzymes | Conversion (%) | Product distribution (%) | | |
|---------------------|----------------|--------------------------|------------------------------|-----------------------------|
| | | 1-tridecene | α -OH-C ₁₄ | β -OH-C ₁₄ |
| CYP-Aa162 | 60.1 ± 2.1 | 16.0 ± 1.2 | 78.9 ± 1.4 | 5.1 ± 0.6 |
| P450 _{BSβ} | 62.8 ± 5.0 | 36.8 ± 3.5 | 30.0 ± 4.2 | 33.2 ± 3.5 |
| CYP-Sm46Δ29 | 73.2 ± 8.9 | 78.4 ± 2.9 | 0.4 ± 0.1 | 21.2 ± 0.9 |
| OleT _{JE} | 74.2 ± 2.9 | 91.8 ± 5.9 | 0.3 ± 0.1 | 7.9 ± 1.5 |

predominantly (78.9 ± 1.4%) the α -hydroxy myristic acid (α -OH-C₁₄), and P450_{BSβ} exhibited approximately even distribution among the three products α -OH-C₁₄, β -OH-C₁₄, and 1-tridecene. In comparison, CYP-Sm46Δ29 and OleT_{JE} showed strong decarboxylation chemoselectivity. For these two enzymes, 1-tridecene was the major product, β -OH-C₁₄ the minor product, while α -OH-C₁₄ only accounted for a negligible proportion of the total products. In all cases, no distal hydroxylated fatty acids beyond C_β position were detected, as opposed to the mixed regioselectivity found with the CYP-MP enzyme [24]. Together, these data strongly support the notion that CYP-Aa162 functions as a P450_{BSβ}-like fatty acid hydroxylase, while CYP-Sm46Δ29 acts as an efficient OleT_{JE}-like decarboxylase, providing another enzyme to the unusual fatty acid oxidative decarboxylation reaction (Additional file 1: Figure S7).

Site-directed mutagenesis of CYP-Aa162 and P450_{BSβ} fatty acid hydroxylases

The active-site sequence alignment of CYP-Aa162 and CYP-Sm46Δ29 with those of P450_{BSβ} and OleT_{JE}

revealed two major residue differences (Additional file 1: Figure S8): the histidine and isoleucine residues in the FFA decarboxylases of OleT_{JE} (H85 and I170) and CYP-Sm46Δ29 (H86 and I171) are replaced by a glutamine and a valine in CYP-Aa162 (Q85 and V170) and P450_{BSβ} (Q85 and V170), respectively. According to the crystal structure of OleT_{JE} (PDB: 4L40) [18], H85 and I170 are positioned at the two sides of the substrate carboxyl group with the distance of 5.1 and 3.4 Å, respectively. Previously, Rude et al. [13] reported an improved decarboxylation activity (~50%) of P450_{BSβ} Q85H variant towards palmitic acid (C₁₆), suggesting an important role of this histidine residue in regulating the decarboxylation chemoselectivity of OleT_{JE}. Grant et al. [20] also proposed mechanisms in which H85 of OleT_{JE} may act as a proton donor to facilitate the protonation of OleT_{JE}-Compound II intermediate (Fe⁴⁺-OH) generated from substrate C-H abstraction and thereby to initiate substrate C-C_α bond scission (i.e., decarboxylation). Moreover, our recent saturation mutagenesis analysis of OleT_{JE} at H85 and I170 sites also confirmed the importance of these two amino acid residues for decarboxylation activity and substrate positioning based on the finding that all H85X (X denotes any natural amino acid) and I170X mutants exhibited abolished decarboxylation activity towards myristic acid [26].

Therefore, in view of the potential key roles of these two residues in regulating decarboxylation process and substrate positioning, we decided to substitute the corresponding amino acids in CYP-Aa162 and P450_{BSβ} with His and Ile, and created the double mutants Aa162/Q85H/V170I and P450_{BSβ}/Q85H/V170I. Their in vitro activities towards a series of free fatty acid substrates (C₁₀-C₂₀) were evaluated along with their corresponding wild types. As a result, the P450_{BSβ}/Q85H/V170I mutant exhibited a general increase in the total substrate conversion ratios compared with its wild type, while Aa162/Q85H/V170I showed variations of increase or decrease in conversion efficiency towards different carbon chain length substrates (Fig. 5c). However, both mutants displayed enhanced decarboxylation activity to the tested substrates to different extents (Fig. 5d). This increase was more prominent in the longer carbon chain length substrates such as C₁₆ palmitic acid (Fig. 5b) than in the shorter carbon chain length substrates such as C₁₂ lauric acid (Fig. 5a). For C₁₂ substrate, a 1.1- and a 0.9-fold increase in 1-undecene production were observed with Aa162/Q85H/V170I and P450_{BSβ}/Q85H/V170I mutant, accounting for a 1.7- and a 1.2-fold increase in the ratio of decarboxylation over hydroxylation activity, respectively (Fig. 5a). For C₁₆ substrate, the production of 1-pentadecene exhibited an increase from undetectable by the wild type CYP-Aa162 to 6.9% by its double mutant Aa162/Q85H/V170I, and an increase of

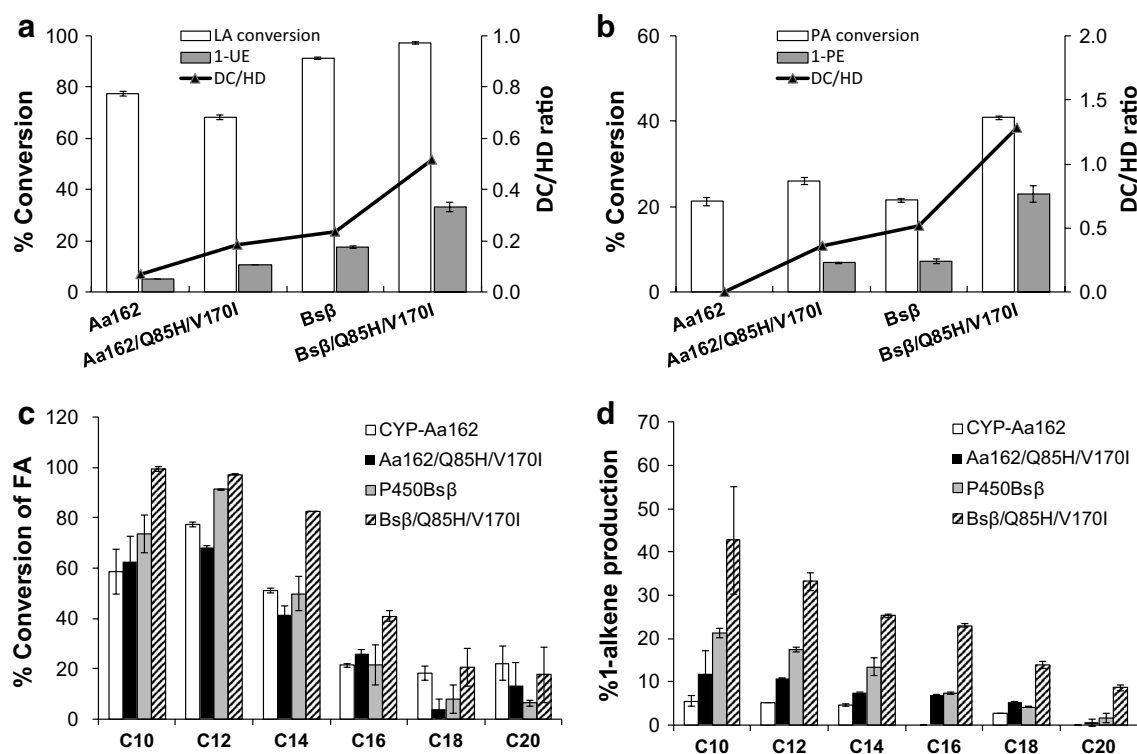


Fig. 5 Fatty acid conversion by the Aa162/Q85H/V170I and P450_{Bsβ}/Q85H/V170I mutants compared to their corresponding wild-type enzymes. The hydroxylation (HD) activity was deduced by subtracting the 1-alkene production (corresponding to DC activity) from the total substrate conversion. **a** Lauric acid (LA) conversion and 1-undecene (1-UE) production; **b** palmitic acid (PA) conversion and 1-pentadecene (1-PE) production; **c** conversion ratios of different carbon chain length fatty acids (C₁₀–C₂₀) and **d** their corresponding 1-alkene production by the indicated enzymes. Results are presented as mean ± SD of duplicated experiments

2.1-fold by the P450_{Bsβ}/Q85H/V170I mutant when compared with its wild type P450_{Bsβ}. The latter increase led to a high decarboxylation versus hydroxylation ratio of around 1.3 in the P450_{Bsβ}/Q85H/V170I mutant, making the 1-alkene the major product. Together, these results demonstrate the important role of the active-site histidine and isoleucine in regulating fatty acid decarboxylation activity of the CYP152 peroxygenases.

Steady-state kinetics of CYP-Aa162 and CYP-Sm46Δ29

To better understand the catalytic properties of CYP-Aa162 fatty acid hydroxylase and CYP-Sm46Δ29 fatty acid decarboxylase, we determined their steady-state kinetic parameters (Table 2) towards their optimal substrates C₁₂ and/or C₁₄ fatty acids. Since CYP-Aa162 mainly catalyzes the hydroxylation of fatty acids, trace amounts of alkene products were undetectable at the beginning of the reaction when initial rates were determined. Therefore, its kinetic constants were derived from the rates of substrate consumption. For CYP-Sm46Δ29, the kinetic constants were specifically determined by 1-alkene formation rates due to its much higher

decarboxylation activity. Interestingly, it was revealed that the kinetic data of both CYP-Aa162 and CYP-Sm46Δ29 towards C₁₂ substrate fit well to a sigmoidal Hill equation with a Hill coefficient value around 2 (Table 2; Additional file 1: Figure S9A, B). This may suggest that the substrate binding pocket of the two P450 enzymes could accommodate more than one C₁₂ molecules and that the binding of one C₁₂ molecule could facilitate the binding of the other to the same P450 enzyme, particularly at low to medium substrate concentrations (10–80 μM). Notably, the kinetic data of CYP-Sm46Δ29 towards C₁₄ substrate exhibited apparent and substantial substrate inhibition (Additional file 1: Figure S9C). When the substrate concentration was in excess of 60 μM, the rate of 1-tridecene formation declined dramatically, but was not completely abolished even at a high concentration of 300 μM. Rather, it flattened off to a low activity, indicating an incomplete inhibition. Estimation of the kinetic parameters for this substrate was therefore deduced from the truncated dataset using Michaelis–Menten equation after removal of the inhibited rates at high substrate concentrations [48]. The apparent k_{cat} value of $62.5 \pm 4.5 \text{ min}^{-1}$ is comparable

Table 2 Kinetic parameters of FFA conversion catalyzed by CYP-Aa162 and CYP-Sm46Δ29

| Enzymes | C ₁₂ ^a | | | | C ₁₄ ^b | | |
|--------------------------|--|----------------------------|---|----------------------|--|----------------------------|---|
| | <i>k</i> _{cat} (min ⁻¹) | <i>K</i> _H (μM) | <i>K</i> _{cat} / <i>K</i> _H (μM ⁻¹ min ⁻¹) | Hill coefficient (n) | <i>k</i> _{cat} (min ⁻¹) | <i>K</i> _m (μM) | <i>K</i> _{cat} / <i>K</i> _m (μM ⁻¹ min ⁻¹) |
| CYP-Aa162 ^c | 46.1 ± 17.1 | 93.1 ± 37.7 | 0.5 | 2.1 ± 0.8 | nd | nd | nd |
| CYP-Sm46Δ29 ^d | 24.5 ± 6.3 | 58.4 ± 19.0 | 0.4 | 2.2 ± 1.0 | 62.5 ± 4.5 | 41.3 ± 5.1 | 1.5 |

nd not determined

^a Data were fitted to Hill equation ($v = V_{\max}[S]^n / (K_H^n + [S]^n)$, *n* Hill coefficient)

^b Substantial substrate inhibition was observed with this substrate. Data shown here were derived from Michaelis–Menten equation after omitting the inhibited rates at high substrate concentrations

^c Initial rates were measured by the amount of substrate consumption per μM enzyme per min

^d Initial rates were measured by the amount of 1-alkene formation per μM enzyme per min. Data (shown as mean ± SE) were calculated using OriginPro 8.0 program

to that of OleT_{JE} towards C₁₄ substrate (71.0 ± 8.4 min⁻¹) [26]. Collectively, these data imply that, to different carbon chain length FFA substrates, the decarboxylase CYP-Sm46Δ29 could present distinct binding modes and therefore display different kinetic behaviors.

Discussion

In this study, we successfully expressed, purified, and biochemically characterized two new CYP152 peroxygenase family members, CYP-Aa162 and CYP-Sm46Δ29, that are capable of decarboxylating straight-chain saturated fatty acids to yield 1-alkenes to different extents. Previously, Chen et al. [49] compared the in vivo alkene production by expressing a His-tagged CYP-Sm46 (there called OleT_{SM}, GenBank Accession Number: WP_009381667, an identical sequence to EKU50422, 453 amino acids) in *S. cerevisiae*, and only observed trace amounts of odd-numbered carbon chain alkenes (C₁₃, C₁₅, and C₁₇) from a 48-h culture of the recombinant yeast cells (total alkene titer 1.4 μg L⁻¹, 40 times lower than that of OleT_{JE} 54.5 μg L⁻¹). In that study, a ‘full-length’ version of CYP-Sm46 was used. No protein expression data were shown, nor was enzymatic characterization performed. Here, our experiment in *E. coli* proved very poor or no soluble expression of the ‘full-length’ version of CYP-Sm46. Translation in bacteria is most commonly initiated at an AUG start codon, which encodes for a methionine. However, in some species, the start codon can be GUG, which within the open reading frame (ORF) would encode for a valine. *Staphylococcus aureus* has been documented to use GUG as an alternative start codon [50]. The use of alternative initiation codons can influence translation efficiency, while incorrect initiation could lead to misfolded and therefore inactive proteins. The initial amino acid sequence of CYP-Sm46 (EKU50422) was most likely mistakenly derived from the usual AUG start codon as it happens to follow a putative Shine–Dalgarno sequence (AGGATG), which may explain why we did not observe decent expression with the original EKU50422

sequence. The later version of the amino acid sequence (CYP-Sm46Δ29) adopted GUG as its start codon (WP_039990689), and a possible Shine–Dalgarno site of 5'-TGGGGG-3' was found 7 base upstream of the putative GUG start codon in the mRNA sequence (Additional file 2). The RBS calculator 2.0 (<http://www.denovodna.com/software/forward>) analysis of the CYP-Sm46 mRNA sequence showed that the GUG has a fivefold higher translation rate (3.3-fold lower total initiation energy ΔG_{Total}) than that of the upstream AUG start codon. In addition, McLaughlin et al. [51] reported the identification of a very strong Shine–Dalgarno complementarity containing five G-C base pairs in the *Staphylococcus aureus* β-lactamase gene. This strong mRNA-16S rRNA binding was proposed to reduce dependence on other initiation factors in the Gram-positive bacteria such as *Bacillus* and *Staphylococcus*. Furthermore, analysis of mRNA sequences of cytochrome P450 family proteins from other *Staphylococcus* species such as *S. agnetis* (GenBank: JPRT01000001.1) and *S. pseudintermedius* (GenBank: CP002439.1) also revealed a similar pattern of the strong 5–6 G-C pairs of Shine–Dalgarno complementarity preceding a GUG start codon. Taken together, we reason that CYP-Sm46Δ29 is most likely to be the native functional form of the protein.

P420 species was generally thought to be an inactive form of cytochrome P450 enzymes [52–54]. Formation of this ‘inactive’ P420 was suggested to involve the protonation of the native cysteine thiolate to a neutral thiol heme ligand [44], the recruitment of a histidine to replace the native cysteinate ligand [45], or other unknown reasons. Either way leads to the failure of forming the thiolate-ligated Fe²⁺ species or to a distorted/weakened heme–thiolate bond, thus underlying the P450 → P420 transition [45]. Most P420 studies were performed with the P450_{BM3} [52, 54] or P450_{cam} [45, 53] monooxygenases. These enzymes employ redox partner system to transfer electrons from NAD(P)H and activate O₂ as the oxidant, whose catalytic activity depends

on the formation of a specific thiolate bond between the heme iron and the absolutely conserved cysteine residue in order to afford an active conformation state [33]. P450 peroxygenases, on the other hand, unlike those monooxygenases, utilize peroxide (such as H_2O_2) to directly convert the heme iron of enzymes to a reactive ferric-hydroperoxy complex ($\text{Fe}^{3+}\text{-OOH}$) via the peroxide shunt pathway [33, 36], therefore bypassing the oxygen activation chemistry and the necessity of forming the thiolate-ligated ferrous-heme species. Whether the failure of observing a P450 species in CYP-Sm46 Δ 29 is due to the instability of the thiolate-ligated P450 species that quickly reverts to a P420 form as with EpoK [43], or an alternative proximal ligand-coordinated species as in P420_{cam} [45], P450 enzymes that undergo peroxide shunt pathway are insensitive to the nature of the proximal ligand as they do not require electron transfer to the heme iron. Peroxide activation can be achieved equally well with, for example, the histidine-ligated hemoproteins [55]. Therefore, as opposed to the generally regarded 'inactive' cytochrome P420 species in the P450 monooxygenases, the peroxygenase 'P420' enzymes can be active. We reason that this difference may explain why we observed no thiolate-ligated P450 ferrous-heme species but a functional CYP-Sm46 Δ 29. Indeed, we observed efficient catalytic activity of CYP-Sm46 Δ 29 in the H_2O_2 system, but not in the H_2O_2 -depleted O_2 /redox proteins/NADH system (Fig. 2b). A minor increase in the activities of CYP-Aa162 and CYP-Sm46 Δ 29 was observed in the catalase-absent redox partner-supported reaction system (Fig. 2b). This increase may reflect the beneficial effect of slow-releasing H_2O_2 from NADH decoupling on the catalytic activity, compared with the batch-added H_2O_2 [24]. However, considering the unique spectroscopic features of the CYP-Sm46 Δ 29, further structural and mechanistic studies are certainly required to gain more detailed understanding of the active-site coordination environment of this enzyme and its catalytic mechanism.

The strict carbon chain length dependence of the decarboxylative activity of CYP-Sm46 Δ 29 is consistent with other identified decarboxylative activities in OleT_{JE} [13, 16, 22], P450_{BSP} [37], and CYP-MP [24], which further emphasizes the importance of substrate identity in controlling the hydroxylation/decarboxylation bifurcation. This substrate identity-dependent chemistry was also manifested in a recent study of OleT_{JE} where only trace amounts (<1–2%) of undesired hydroxyl side products were generated when aromatic carboxylic acids were used as substrates [29]. Our finding that low alkene production in CYP-Aa162 is accompanied with a high percentage of α -hydroxyl product is also consistent with the notion that $\text{C}_\beta\text{-H}$ rather than $\text{C}_\alpha\text{-H}$ abstraction is a prerequisite for initiation of fatty acid decarboxylation pathway.

However, this could not be the sole determining factor as CYP-MP produced predominantly the β -OH fatty acid but only a meager amount of alkenes [24]. For OleT_{JE}, it was proposed that His85 could facilitate the decarboxylation pathway through providing proton to the $\text{Fe}^{4+}\text{-OH}$ (compound II) intermediate to restore a water-bound $\text{Fe}^{3+}\text{-OH}_2$ species [18, 20]. An active-site histidine may also help with the precise substrate positioning required for the decarboxylation pathway [26]. In the absence of an active-site histidine, $\cdot\text{OH}$ rebound would be the prevalent pathway, leading to accumulated hydroxyl fatty acids, such as the case with CYP-MP [24], P450_{BSP} [13], and CYP-Aa162 in this study. Our site-directed mutagenesis analysis of CYP-Aa162 and P450_{BSP} confirmed the importance of this residue in regulating decarboxylation selectivity. However, the introduction of this histidine residue did not fully reverse the chemoselectivity of either CYP-MP [24] or CYP-Aa162 (Fig. 5), albeit an increase in the decarboxylation activity, hydroxylation was still the major chemistry of CYP-Aa162/Q85H/V170I. This implies that more structural and electronic requirements need to be satisfied to be a fatty acid decarboxylase.

Makris and coworkers [19, 20] recently confirmed that OleT_{JE} catalysis is initiated by the formation of an iron(IV)-oxo cation radical (compound I). The fatty acid decarboxylation bifurcation is believed to begin with a regio-specific $\text{C}_\beta\text{-H}$ abstraction followed by a single-electron transfer from either a substrate carboxylate group or an additional electron from the C_β position to the incipient compound II, resulting in the generation of a substrate diradical or a substrate carbocation, respectively, to fulfill C-C_α bond scission and give rise to the terminal alkene products. Our data here together with others [13, 18–20, 23, 24] suggest that substrate $\text{C}_\beta\text{-H}$ abstraction, chain length-dependent precise positioning at the active site, relative intrinsic stability of the enzyme/ $\text{Fe}^{4+}\text{-OH}$ intermediate (compound II), and the competition between $\cdot\text{OH}$ rebound and abstraction of an additional substrate electron by compound II are among the decarboxylation bifurcation determinants to ensure a desaturation reaction. Given that site-directed mutagenesis did not fully boost the decarboxylation activity of CYP-Aa162, alternative approaches such as directed evolution may represent an attractive method for engineering improved alkene formation activity towards, especially, particular chain length substrates, and for thorough understanding of the enzyme structure–function relationship.

A majority of P450 catalyses follow simple Michaelis–Menten kinetics based on a single active site for the substrate–enzyme interaction [56]. However, there are growing cases that non-Michaelis–Menten kinetics were observed for some P450 reactions [48, 57–59]. In the

latter cases, the non-classical kinetics apparently results from allosteric effects that commonly lead to a sigmoidal velocity curve. The Hill equation can be used to indicate cooperative kinetics. Indeed, several studies have found that some P450s are able to fit into its active site with large molecules such as cyclosporine [60] or two substrates at once [57]. The two substrates can be the same or different molecules allowing the homotropic or heterotropic cooperative kinetics, respectively. Other examples of cooperative catalysis were found with P450_{SP α} [61, 62] and P450_{BS β} [62, 63] where short-chain length fatty acids (such as heptanoic acid or hexanoic acid) could act as 'decoy molecules' to facilitate the binding of non-natural substrates (such as styrene) and their oxidation by these P450 peroxygenases. In this study, cooperative binding of C₁₂ lauric acid substrate to CYP-Aa162 and CYP-Sm46 Δ 29 enzymes was observed with a Hill coefficient of ~2 (Table 1). The smaller k_{cat} and k_{cat}/K_m values of CYP-Sm46 Δ 29 towards C₁₂ lauric acid ($24.5 \pm 6.3 \text{ min}^{-1}$ and $0.4 \mu\text{M}^{-1} \text{ min}^{-1}$) than those towards C₁₄ myristic acid ($62.5 \pm 4.5 \text{ min}^{-1}$ and $1.5 \mu\text{M}^{-1} \text{ min}^{-1}$) may appear to be contradictory to the qualitative substrate specificity results (Fig. 2) which demonstrated higher conversion efficiency of C₁₂ over C₁₄ by this enzyme. We reason that this inconsistency may stem from the substrate inhibition of this enzyme by the high substrate concentration of C₁₄ (200 μM substrate was used for the substrate specificity profiling assay).

Conclusions

In this study, we have characterized two new CYP152 peroxygenases with regard to their spectroscopic characteristics, substrate specificity, decarboxylation/hydroxylation chemoselectivity, and kinetics. Our data demonstrate that CYP-Sm46 Δ 29 works as an efficient OleT_{IE}-like fatty acid decarboxylase, while CYP-Aa162 acts as a P450_{BS β} -like fatty acid hydroxylase with marginal decarboxylation chemoselectivity. Furthermore, CYP-Sm46 Δ 29 was found to be catalytically active without forming a stable P450 species. Its decarboxylation activity exhibited strict carbon chain length dependence, suggesting the requirement of precise active-site positioning of substrates to be decarboxylated. Moreover, towards different carbon chain length fatty acids, CYP-Sm46 Δ 29 undertook different kinetic behaviors (cooperative or substrate inhibition), further stressing the importance and impact of elaborate coordination of substrate within the substrate binding pocket. Taken together, our findings could provide more opportunities for further understanding the unique catalytic mechanism employed by CYP152 fatty acid decarboxylases and also serve as a guide for future bioengineering of the

enzymes for improved alkene-producing activity of different carbon chain length substrates.

Methods

Materials

Fatty acid substrates, terminal alkene authentic standards, α -hydroxy myristic acid, β -hydroxy myristic acid, and *N,O*-bis(trimethylsilyl)trifluoroacetamide (BSTFA) with 1% trimethylchlorosilane were purchased from TCI (Shanghai, China). Catalase from bovine liver (# C1345) was purchased from Sigma-Aldrich (St. Louis, MO, USA). One unit is defined, as described in the manufacturer's instruction, to decompose 1.0 μmol of H₂O₂ min⁻¹ at pH 7.0 at 25 °C, while the H₂O₂ concentration falls from 10.3 to 9.2 mM, measured by the rate of decrease of A₂₄₀. NADH and antibiotics were obtained from Solarbio (Beijing, China). Other chemicals were purchased from Ameresco (Solon, OH, USA) or Sigma-Aldrich (St. Louis, MO, USA). Molecular cloning kits, such as High Purity Plasmid Miniprep Kit and Wizard SV Gel and PCR Clean-up System, were purchased from TSINGKE Biotech (Beijing, China) and Promega (Madison, WI, USA), respectively. Oligonucleotides and codon-optimized genes were synthesized by Genewiz (Suzhou, China). The *Pfu* DNA polymerases and all restriction endonucleases were obtained from Takara (Dalian, China). Ni-NTA resin used for protein purification was purchased from Qiagen (Valencia, CA, USA). The FlexiRun™ pre-mixed gel solution for SDS-PAGE was obtained from MDBio, Amicon Ultra centrifugal filters from Millipore (Billerica, MA, USA), and PD-10 desalting columns from GE Healthcare (Piscataway, NJ, USA).

Molecular cloning

The gene sequences encoding CYP-Aa162 from *Alicyclobacillus acidocaldarius* LAA1 (CYP152A8, GenBank Accession Number: WP_008340313) and CYP-Sm46 from *Staphylococcus massiliensis* strain S46 (CYP152L2, GenBank Accession Number: Eku50422) were, respectively, codon-optimized and synthesized by Genewiz (Suzhou, China), and cloned into the expression vector pET28b between NdeI/XhoI restriction sites with a hexahistidine tag at the N terminus for expression in *E. coli* BL21 (DE3). The truncated *CYP-Sm46 Δ 29* gene (WP_039990689) was PCR-amplified from the initial construct of pET28b-*CYP-Sm46* using *Pfu* DNA polymerase and then subcloned into pET28b vector using the same restriction sites as above. The generation of double mutant gene constructs of Aa162/Q85H/V170I and P450_{BS β} /Q85H/V170I was achieved by site-directed mutagenesis via overlap extension PCR [64]. The sequences of primers used in this study are listed in Additional file 3: Table S1. All plasmid constructs were confirmed by DNA sequencing at Sangon

Biotech (Shanghai, China). Upon sequence verification, plasmids were used to transform *E. coli* BL21 (DE3) for protein expression.

Heterologous expression and purification

The *E. coli* BL21 (DE3) cells transformed with pET28b-CYP-Sm46Δ29, pET28b-CYP-Aa162, or the Q85H/V170I double mutant constructs were grown overnight at 37 °C with shaking at 220 rpm in LB medium containing 50 μg mL⁻¹ kanamycin. The overnight culture was used as a seed culture to inoculate (1:100 dilution) 1–3 L of modified terrific broth containing 4% glycerol, 1 mM thiamine, trace metals [16], and the corresponding antibiotics. Cells were then grown at 37 °C for 3–4 h until the optical density at 600 nm (OD₆₀₀) reached ~0.6, at which point δ-aminolevulinic acid (0.5 mM final concentration) was supplemented and the expression of CYP-Sm46Δ29 was induced by the addition of 0.2 mM isopropyl-β-D-thiogalactopyranoside (IPTG). Cells were further cultured for 24 h at 18 °C before being harvested by centrifugation at 6000 rpm, 4 °C. The cell pellet was frozen at –80 °C until required.

Purification of the His-tagged protein was carried out as described by Liu et al. [16] with minor modifications. All protein purification steps were performed at 4 °C. Specifically, the cell pellets were thawed and resuspended in 40 mL lysis buffer (50 mM NaH₂PO₄, 300 mM NaCl, 10% glycerol, and 10 mM imidazole, pH 8.0) through vortexing. After cell disruption by ultrasonication, the cell lysate was centrifuged at 12,000×g for 30 min to remove cellular debris. To the clarified cell lysate, 1 mL of Ni–NTA resin was added and gently mixed at 4 °C for 1 h. The slurry was then loaded onto an empty column and washed with approximately 100 mL of wash buffer (50 mM NaH₂PO₄, 300 mM NaCl, 10% glycerol, and 20 mM imidazole, pH 8.0) until no proteins were detectable in flowthrough. The bound target proteins were eluted with elution buffer (50 mM NaH₂PO₄, 300 mM NaCl, 10% glycerol, and 250 mM imidazole, pH 8.0). The eluates were pooled and concentrated with an Amicon Ultra centrifugal filter (30 kDa cutoff). Imidazole contained in the protein eluates was removed by ultrafiltration and buffer exchange on a PD-10 column into storage buffer (50 mM NaH₂PO₄, 300 mM NaCl, 10% glycerol, pH 7.4). The final purified protein was flash-frozen with liquid nitrogen and stored at –80 °C for later use.

UV–visible spectroscopic characterization of CYPs

Analysis of the UV–visible spectroscopic properties of the His-tagged CYP-Aa162 and CYP-Sm46Δ29 was performed on a Cary 60 UV–visible spectrophotometer (Varian, UK). For preparation of the dithionite-reduced ferrous-CO complex of each enzyme, carbon monoxide gas was

slowly bubbled into a solution of purified ferric enzyme (~4–7 μM) in 50 mM NaH₂PO₄, 300 mM NaCl, 10% glycerol, pH 7.4, immediately followed by sufficient reduction of the protein with sodium dithionite (1–3 mg) [65]. The optical absorption spectra of the ferric and ferrous-CO forms of each enzyme were recorded, respectively, before and after the addition of sodium dithionite. The CO-bound reduced difference spectrum was obtained according to the previous report [66]. In order to record the spectra in the redox partners/NAD(P)H/CO system, lauric acid (~0.7 mM) was pre-incubated with the cytochrome proteins for 5 min at 28 °C before the absorbance of ferric forms was recorded. Then, to the substrate-bound protein solution was added the CamAB/NADH (for CYP-Aa162 and CYP-Sm46Δ29) or NADPH (for the self-sufficient P450_{BM3}) cofactors to initiate a flavin-to-heme electron transfer. Spectra of the CO-bound NAD(P)H-reduced forms of the P450 enzymes were subsequently recorded. The protein concentration was determined by the extinction coefficient of ε_{422 nm} = 104 mM⁻¹ cm⁻¹ as determined using the pyridine hemochromogen method [67]. The typical methodology for determination of the P450 functional concentration using ε_{450–490 nm} [66] was abandoned due to lack of the P450 content in the CYP-Sm46Δ29 spectra.

In vitro enzymatic assay

Typical assays containing 1.5 μM of each CYP enzyme (CYP-Sm46Δ29 or CYP-Aa162 or their mutant), 200 μM fatty acid substrate (one of the C₁₀–C₂₀ FFAs prepared from a 20 mM stock solution in DMSO), and 220 μM H₂O₂ in 200 μL of storage buffer were carried out at 28 °C for 2 h. Reactions were quenched by the addition of 20 μL of 10 M HCl. Heptadecanoic acid was then added as the internal standard, and the mixture was extracted by 200 μL ethyl acetate. Following extraction, the organic phase was collected and analyzed by gas chromatography (GC) as described below.

For detection of the volatile C₉ nonene product generated from C₁₀ fatty acid decarboxylation, 500 μL of the reaction system containing 200 μM C₁₀ fatty acid substrate, 220 μM H₂O₂, 2.0 μM of enzyme, and 200 μM C₇ 1-heptene as the internal standard in a 1.5 mL polytetrafluorethylene (PTFE) septum-sealed glass bottles was incubated at 28 °C for 2 h with shaking at 300 rpm. The reactions were then placed on ice and subjected to headspace sampling using a gas-tight Hamilton syringe for GC–MS analysis as described below. The standard curve of nonene was obtained by incubating different concentrations of the authentic nonene standard under the same condition as the reactions without enzyme followed by the same GC–MS analysis. After headspace sampling, the reactions were immediately mixed with ethyl acetate and the internal standard heptadecanoic acid and extracted

as described above for the analysis of the remaining C_{10} substrates. With every tested substrate (C_{10} – C_{20} FFAs), a reaction without H_2O_2 was used as the control for the initial substrate concentration.

Steady-state kinetic analysis

To determine the P450 kinetic parameters, 0.1–0.5 nM of enzyme was incubated with varying concentrations of substrate (C_{12} or C_{14}) at 28 °C in a 1 mL reaction system (50 mM NaH_2PO_4 , 300 mM NaCl, pH 7.4, 10% glycerol) supplemented with an excess amount of H_2O_2 as a cofactor. Aliquots (200 μ L) of reactions were removed and quenched at specific time points (usually at 0, 1, 3, and 5 min) by adding 1/10 volume of 1 M HCl. Heptadecanoic acid was then added as the internal standard. Subsequent sample preparation was performed (as above) for GC analysis (as below). Initial rates were calculated from either the substrate consumption for CYP-Aa162 or the 1-alkene production for CYP-Sm46 Δ 29. Kinetic analyses were performed using OriginPro 8.0 program.

Gas chromatography (GC) and GC–MS

The GC analytical method for hydrocarbon and fatty acid samples was adapted from Guan et al. [68]. The analyses were performed on an Agilent 7890B gas chromatograph equipped with a capillary column HP-INNOWAX (Agilent Technologies, Santa Clara, CA, USA; cross-linked polyethylene glycerol, i.d. 0.25 μ m film thickness, 30 m by 0.25 mm). The helium flow rate was set to 1 mL per min. The oven temperature was controlled initially at 40 °C for 4 min, then increased at the rate of 10 °C min^{-1} to 280 °C, and held for 5 min. The injecting temperature was set to 280 °C with the injection volume of 1 μ L under splitless injection conditions. The retention times and signal intensity of fatty acids and alkenes were determined by analyzing and comparing with known authentic fatty acids (C_{10} – C_{20}), 1-alkenes (C_{11} – C_{19}), and 1-heptadecanoic acid standards [16]. For GC–MS, the gas chromatography equipment was coupled to an Agilent 5975C MSD single quadrupole mass spectrometer operated under electron ionization mode at 70 eV in the scan range of 50–500 m/z . For detection of the hydroxyl fatty acid products, as only authentic standards of α - and β -hydroxy myristic acids were obtained, samples extracted from the C_{14} myristic acid reactions were derivatized with an equal volume of *N,O*-bis(trimethylsilyl)trifluoroacetamide (BSTFA) with 1% trimethylchlorosilane at 72 °C for 15 min prior to GC–MS analysis. The GC–MS analysis followed the protocol developed by Rude et al. [13], except for using the Agilent J&W DB-5MS column (i.d. 0.25 μ m film thickness, 50 m by 0.25 mm). Peak identity was determined by comparison of retention time and fragmentation pattern

with the authentic standard compounds where available and to the National Institute of Standards and Technology, USA mass spectral database. From the reactions using myristic acid as a substrate, we found that the sum of all products (1-tridecene, α - and β -hydroxy myristic acids) almost accurately accounts for at least 99% of the substrate consumption. In addition, as only a minimal level of H_2O_2 relative to fatty acid substrate (slightly more than 1:1 molar ratio) was used, no overly oxidized products (such as ketones, di-hydroxyl fatty acids) were observed within the detection limit. Therefore, we quantified the percentage of hydroxylated products for all substrates by subtraction of the 1-alkene production from the total substrate consumption unless otherwise stated. For detection of nonene product from the C_{10} fatty acid reactions, 600 μ L of the reaction headspace sample was injected into the GC–MS system using a Hamilton needle syringe. The oven temperature program was as follows: 40 °C for 2 min, then 5 °C per min to 100 °C, and held for 2 min. Quantification of the nonene product was based on the standard curve and reaction controls.

Additional files

Additional file 1: Figure S1. Protein sequence alignment of CYP-Aa162 from *A. acidocaldarius* (GenBank Accession Number: WP_008340313), P450_{B5B} from *Bacillus subtilis* str. 168 (GenBank Accession Number: NP_388092), OleT_{JE} from *Jeotgalicoccus* sp. ATCC 8456 (GenBank Accession Number: ADW41779), CYP-Sm46 (labelled as Sm46 extended) from *Staphylococcus massiliensis* S46 (GenBank Accession Number: Eku50422), CYP-Sm46 Δ 29 (labelled as Sm46 Δ 29) from *S. massiliensis* (GenBank Accession Number: WP_039990689) and cytochrome P450 enzymes from other *Staphylococcus* species such as *S. agnetis* (GenBank Accession Number: KFE42911), *S. delphini* (GenBank Accession Number: WP_019165531), *S. intermedius* (GenBank Accession Number: WP_019167377) and *S. pseud-intermedius* HKU10-03 (GenBank Accession Number: ADV05454). **Figure S2.** SDS-PAGE showing the purified His-tagged CYP-Aa162 (lane A) and CYP-Sm46 Δ 29 (lane S). Molecular sizes of the marker bands (lane M), from top to bottom, are 180, 135, 100, 75, 63, 48, 35 and 25 kDa respectively. **Figure S3.** The UV-visible spectra of CYP-Sm46 Δ 29 (5 μ M) under different conditions. (A) The purified CYP-Sm46 Δ 29 was diluted in 50 mM Na_3PO_4 (pH 7.4) buffer containing 300 mM NaCl and 10% glycerol. Spectra are shown for the oxidized ferric form of the enzyme (orange line) and the ferrous-CO complex reduced by the indicated amount of $Na_2S_2O_4$. (B) The purified CYP-Sm46 Δ 29 was diluted in 50 mM Na_3PO_4 buffer containing 300 mM NaCl and 10% glycerol with different buffer pH as indicated. Then the absorption spectra were recorded respectively for the oxidized ferric form and the ferrous-CO adduct reduced by 10 mM $Na_2S_2O_4$. The protein precipitates at buffer pH lower than 7.0. (C) A molar excess (600 μ M) of C_{12} lauric acid was pre-incubated with the enzyme at room temperature for 5 min before the absorption spectra were recorded. Binding of C_{12} FA did not seem to induce an apparent spin-state transition of the ferric heme. The Soret peak of the C_{12} -bound ferrous-CO adduct of the enzyme was still detected at 420 nm. **Figure S4.** UV-visible spectra of the self-sufficient monooxygenase P450_{BM3}. The substrate-bound ferric form of P450_{BM3} (solid line) shows a Soret maximum at ~416 nm with undistinguishable β -band and a weaker α -band at 570 nm. The reduced ferrous-CO form of P450_{BM3} (dashed line) generated by the subsequent NADPH-initiated electron transfer features a shifted Soret peak to 448 nm. **Figure S5.** Effect of decoupling NADH oxidation and electron transfer on the catalytic conversion of lauric acid (LA) by CYP-Aa162 and CYP-Sm46 Δ 29. The reactions contained 0.2 mM LA, 2.0 μ M CYP-Aa162 (or

CYP-Sm46Δ29), 3.0 μM putidaredoxin reductase (PdR), 1 mM NADH in the absence and presence of 1200 U mL⁻¹ catalase (CatI). By subtracting putidaredoxin (Pdx) from the reaction system, the NADH oxidation was mandatorily decoupled from the Class I electron transfer chain to P450 enzymes. Any catalytic activity observed should be supported by the H₂O₂ generated from NADH oxidation and O₂ reduction. The percentage conversion of LA was determined by calculating the substrate consumption based on GC analysis. Results shown are mean ± SD of duplicated experiments. **Figure S6.** The ratios of free fatty acid (FFA) decarboxylation (DC) over hydroxylation (HD) by CYP-Sm46Δ29 against different FFA substrates. The decarboxylation activity was measured by detecting the 1-alkene yield using GC analytical method. The hydroxylation activity was estimated by subtracting the alkene production from the total substrate conversion. This indirect but more convenient method was validated with C₁₄ myristic acid substrate by direct measurement of the BSTFA/TMCS derivatized hydroxylation products. Results are shown as mean ± SD of duplicated experiments. **Figure S7.** Phylogenetic tree for CYP-Aa162, CYP-Sm46Δ29 and other CYP152 family members. The sequences were aligned using ClustalW. The Neighbor-joining Tree was generated using MEGA 7.0 package. Bootstrap values shown next to the branches were computed from 1000 bootstrap tests. CYP-Sm46 was found most closely related to the P450 fatty acid decarboxylase OleT_{JE} (CYP152L1), while CYP-Aa162 (CYP152A8) is much closer to the P450 fatty acid hydroxylase P450_{B5B} (CYP152A1). **Figure S8.** Protein sequence alignment of OleT_{JE}, CYP-Sm46Δ29, CYP-Aa162 and P450_{B5B}. *: the only two residues that are distinct in the active sites of these four P450 peroxygenases, which are proposed to be important for product distribution; #: the key catalytic residue. **Figure S9.** Kinetic curves of CYP-Aa162 and CYP-Sm46Δ29 against their optimal fatty acid substrates. (A) C₁₂ lauric acid substrate consumption rates by CYP-Aa162 were fitted to Hill equation; (B) 1-undecene formation rates by CYP-Sm46Δ29 were fitted to Hill equation; (C) Solid line: the plot of 1-tridecene formation rates by CYP-Sm46Δ29 as a function of increasing C₁₄ myristic acid concentrations, demonstrating substantial substrate inhibition. Dotted line: a hyperbolic curve fitted with Michaelis-Menten equation after truncating the inhibited rates at high C₁₄ substrate concentrations. The steady state kinetic parameters were calculated using OriginPro 8.0 and are summarized in Table 2.

Additional file 2. The original gene sequence of CYP-Sm46, and the codon-optimized gene sequences of CYP-Sm46 and CYP-Aa162, as well as their corresponding amino acid sequences.

Additional file 3: Table S1. Primers used for cloning and site-directed mutagenesis.

Abbreviations

CYP or P450: cytochrome P450 enzyme; FFA: free fatty acid; LS: low-spin heme iron; CamAB: the P450cam redox partner proteins including putidaredoxin reductase and putidaredoxin; LA: lauric acid; 1-UE: 1-undecene; TB: terrific broth; IPTG: isopropyl β-D-1-thiogalactopyranoside; Ni-NTA: nickel-nitrilotriacetic acid resin; GC-MS: gas chromatography-mass spectrometry; DC: decarboxylation; HD: hydroxylation.

Authors' contributions

SL, LF, SC, FL, HX, and JX conceived and designed the study. HX, LN, WY, BF, WY, and CW performed the experiments and analyzed the results. HX, LF, and SL wrote the manuscript. All authors read and approved the final manuscript.

Author details

¹ Shandong Provincial Key Laboratory of Synthetic Biology, Qingdao Institute of Bioenergy and Bioprocess Technology, Chinese Academy of Sciences, No. 189 Songling Road, Qingdao 266101, Shandong, China. ² CAS Key Laboratory of Biofuels, Qingdao Institute of Bioenergy and Bioprocess Technology, Chinese Academy of Sciences, No. 189 Songling Road, Qingdao 266101, Shandong, China. ³ Single-Cell Center, Qingdao Institute of Bioenergy and Bioprocess Technology, Chinese Academy of Sciences, No. 189 Songling Road, Qingdao 266101, Shandong, China. ⁴ University of Chinese Academy

of Sciences, Beijing 100049, China. ⁵ Total Refinery and Chemistry, SDR/Biofuels, Tour Coupole, 2, Pl. Jean Millier, 92400 Courbevoie, France.

Acknowledgements

We thank Prof. Zhiqi Cong at Qingdao Institute of Bioenergy and Bioprocess Technology, Chinese Academy of Sciences for his valuable discussion and suggestions. We are also grateful to Dr. Yousong Ding at University of Florida and Prof. Thomas Pochapsky at Rutgers University for their kind gifts of the plasmids for expression of P450_{BM3} and CamAB, respectively.

Competing interests

The authors declare that they have no competing interests.

Availability of supporting data

All data generated or analyzed during this study are included in this manuscript (and its Additional files 1, 2, 3).

Consent for publication

Not applicable.

Ethics approval and consent to participate

Not applicable.

Funding

This work was supported by the National Science Foundation of China (NSFC 31422002 and 31770844) and the Natural Science Foundation of Shandong Province, Grant JQ201407. This study was also carried out in the framework of the Collaboration Agreement between TOTAL and QIBEBT-CAS (Qingdao Institute of Bioenergy and Bioprocess Technology, Chinese Academy of Sciences).

Publisher's Note

Springer Nature remains neutral with regard to jurisdictional claims in published maps and institutional affiliations.

Received: 21 February 2017 Accepted: 28 August 2017

Published online: 07 September 2017

References

- Denisov IG, Makris TM, Sligar SG, Schlichting I. Structure and chemistry of cytochrome P450. *Chem Rev.* 2005;105:2253–77.
- Bernhardt R. Cytochromes P450 as versatile biocatalysts. *J Biotechnol.* 2006;124:128–45.
- Hrycay EG, Bandiera SM. The monooxygenase, peroxidase, and peroxygenase properties of cytochrome P450. *Arch Biochem Biophys.* 2012;522:71–89.
- Grogan G. Cytochromes P450: exploiting diversity and enabling application as biocatalysts. *Curr Opin Chem Biol.* 2011;15:241–8.
- Guengerich FP, Munro AW. Unusual cytochrome p450 enzymes and reactions. *J Biol Chem.* 2013;288:17065–73.
- Furge LL, Guengerich FP. Cytochrome P450 enzymes in drug metabolism and chemical toxicology: an introduction. *Biochem Mol Biol Educ.* 2006;34:66–74.
- Steen EJ, Kang Y, Bokinsky G, Hu Z, Schirmer A, McClure A, Del Cardayre SB, Keasling JD. Microbial production of fatty-acid-derived fuels and chemicals from plant biomass. *Nature.* 2010;463:559–62.
- Liao W, Heijungs R, Huppes G. Natural resource demand of global biofuels in the anthropocene: a review. *Renew Sustain Energy Rev.* 2012;16:996–1003.
- Dutta K, Daverey A, Lin J-G. Evolution retrospective for alternative fuels: first to fourth generation. *Renew Energy.* 2014;69:114–22.
- Timilsina GR. Biofuels in the long-run global energy supply mix for transportation. *Philos Trans A Math Phys Eng Sci.* 2014;372:20120323.
- Schirmer A, Rude MA, Li X, Popova E, del Cardayre SB. Microbial biosynthesis of alkanes. *Science.* 2010;329:559–62.
- Choi YJ, Lee SY. Microbial production of short-chain alkanes. *Nature.* 2013;502:571–4.

13. Rude MA, Baron TS, Brubaker S, Alibhai M, Del Cardayre SB, Schirmer A. Terminal olefin (1-alkene) biosynthesis by a novel p450 fatty acid decarboxylase from *Jeotgalicoccus* species. *Appl Environ Microbiol*. 2011;77:1718–27.
14. Rui Z, Li X, Zhu X, Liu J, Domigan B, Barr I, Cate JH, Zhang W. Microbial biosynthesis of medium-chain 1-alkenes by a nonheme iron oxidase. *Proc Natl Acad Sci USA*. 2014;111:18237–42.
15. Gu L, Wang B, Kulkarni A, Gehret JJ, Lloyd KR, Gerwick L, Gerwick WH, Wipf P, Hakansson K, Smith JL, Sherman DH. Polyketide decarboxylative chain termination preceded by o-sulfonation in curacin A biosynthesis. *J Am Chem Soc*. 2009;131:16033–5.
16. Liu Y, Wang C, Yan J, Zhang W, Guan W, Lu X, Li S. Hydrogen peroxide-independent production of alpha-alkenes by OleTJE P450 fatty acid decarboxylase. *Biotechnol Biofuels*. 2014;7:28.
17. Rui Z, Harris NC, Zhu X, Huang W, Zhang W. Discovery of a Family of Desaturase-Like Enzymes for 1-Alkene Biosynthesis. *ACS Catal*. 2015;5:7091–4.
18. Belcher J, McLean KJ, Matthews S, Woodward LS, Fisher K, Rigby SE, Nelson DR, Potts D, Baynham MT, Parker DA, et al. Structure and biochemical properties of the alkene producing cytochrome P450 OleTJE (CYP152L1) from the *Jeotgalicoccus* sp. 8456 bacterium. *J Biol Chem*. 2014;289:6535–50.
19. Grant JL, Hsieh CH, Makris TM. Decarboxylation of fatty acids to terminal alkenes by cytochrome P450 compound I. *J Am Chem Soc*. 2015;137:4940–3.
20. Grant JL, Mitchell ME, Makris TM. Catalytic strategy for carbon-carbon bond scission by the cytochrome P450 OleT. *Proc Natl Acad Sci USA*. 2016;113:10049–54.
21. Zachos I, Gassmeyer SK, Bauer D, Sieber V, Hollmann F, Kourist R. Photobiocatalytic decarboxylation for olefin synthesis. *Chem Commun (Camb)*. 2015;51:1918–21.
22. Dennig A, Kuhn M, Tassoti S, Thiessenhusen A, Gilch S, Bulter T, Haas T, Hall M, Faber K. Oxidative decarboxylation of short-chain fatty acids to 1-alkenes. *Angew Chem Int Ed Engl*. 2015;54:8819–22.
23. Faponle AS, Quesne MG, de Visser SP. Origin of the regioselective fatty-acid hydroxylation versus decarboxylation by a cytochrome p450 peroxxygenase: what drives the reaction to biofuel production? *Chemistry (Easton)*. 2016;22:5478–83.
24. Amaya JA, Rutland CD, Makris TM. Mixed regioselectivity compromises alkene synthesis by a cytochrome P450 peroxxygenase from *Methylobacterium populi*. *J Inorg Biochem*. 2016;158:11–6.
25. Yan J, Liu Y, Wang C, Han B, Li S. Assembly of lipase and P450 fatty acid decarboxylase to constitute a novel biosynthetic pathway for production of 1-alkenes from renewable triacylglycerols and oils. *Biotechnol Biofuels*. 2015;8:34.
26. Fang B, Xu H, Liu Y, Qi F, Zhang W, Chen H, Wang C, Wang Y, Yang W, Li S. Mutagenesis and redox partners analysis of the P450 fatty acid decarboxylase OleT_{JE}. *Sci Rep*. 2017;7:44258.
27. Hsieh CH, Huang X, Amaya JA, Rutland CD, Keys CL, Groves JT, Austin RN, Makris TM. The enigmatic P450 decarboxylase OleT is capable of, but evolved to frustrate, oxygen rebound chemistry. *Biochemistry*. 2017;56:3347–57.
28. Matthews S, Belcher JD, Tee KL, Girvan HM, McLean KJ, Rigby SE, Levy CW, Leys D, Parker DA, Blankley RT, Munro AW. Catalytic determinants of alkene production by the cytochrome P450 peroxxygenase OleTJE. *J Biol Chem*. 2017;292:5128–43.
29. Wang JB, Lonsdale R, Reetz MT. Exploring substrate scope and stereoselectivity of P450 peroxxygenase OleTJE in olefin-forming oxidative decarboxylation. *Chem Commun (Camb)*. 2016;52:8131–3.
30. Dennig A, Kurakin S, Kuhn M, Dordic A, Hall M, Faber K. Enzymatic oxidative tandem decarboxylation of dioic acids to terminal dienes. *Eur J Org Chem*. 2016;2016:3473–7.
31. Hsieh CH, Makris TM. Expanding the substrate scope and reactivity of cytochrome P450 OleT. *Biochem Biophys Res Commun*. 2016;476:462–6.
32. Schlichting I, Berendzen J, Chu K, Stock AM, Maves SA, Benson DE, Sweet RM, Ringe D, Petsko GA, Sligar SG. The catalytic pathway of cytochrome p450cam at atomic resolution. *Science*. 2000;287:1615–22.
33. Hrycay EG, Bandiera SM. Monooxygenase, peroxidase and peroxxygenase properties and reaction mechanisms of cytochrome P450 enzymes. *Adv Exp Med Biol*. 2015;851:1–61.
34. Matsunaga I, Sumimoto T, Ueda A, Kusunose E, Ichihara K. Fatty acid-specific, regioselective, and stereospecific hydroxylation by cytochrome P450 (CYP152B1) from *Sphingomonas paucimobilis*: substrate structure required for alpha-hydroxylation. *Lipids*. 2000;35:365–71.
35. Matsunaga I, Ueda A, Fujiwara N, Sumimoto T, Ichihara K. Characterization of the ybdT gene product of *Bacillus subtilis*: novel fatty acid beta-hydroxylating cytochrome P450. *Lipids*. 1999;34:841–6.
36. Montellano PROd. *Cytochrome P450: structure, mechanism, and biochemistry*. 4th ed. New York: Springer International Publishing; 2015.
37. Lee DS, Yamada A, Sugimoto H, Matsunaga I, Ogura H, Ichihara K, Adachi S, Park SY, Shiro Y. Substrate recognition and molecular mechanism of fatty acid hydroxylation by cytochrome P450 from *Bacillus subtilis*. Crystallographic, spectroscopic, and mutational studies. *J Biol Chem*. 2003;278:9761–7.
38. Chang MCY, Eachus RA, Trieu W, Ro D-K, Keasling JD. Engineering *Escherichia coli* for production of functionalized terpenoids using plant P450s. *Nat Chem Biol*. 2007;3:274–7.
39. Petersen TN, Brunak S, von Heijne G, Nielsen H. SignalP 4.0: discriminating signal peptides from transmembrane regions. *Nat Methods*. 2011;8:785–6.
40. Krogh A, Larsson B, von Heijne G, Sonnhammer EL. Predicting transmembrane protein topology with a hidden Markov model: application to complete genomes. *J Mol Biol*. 2001;305:567–80.
41. Kall L, Krogh A, Sonnhammer EL. A combined transmembrane topology and signal peptide prediction method. *J Mol Biol*. 2004;338:1027–36.
42. Girvan HM, Marshall KR, Lawson RJ, Leys D, Joyce MG, Clarkson J, Smith WE, Cheesman MR, Munro AW. Flavocytochrome P450 BM3 mutant A264E undergoes substrate-dependent formation of a novel heme iron ligand set. *J Biol Chem*. 2004;279:23274–86.
43. Ogura H, Nishida CR, Hoch UR, Perera R, Dawson JH, Ortiz de Montellano PR. EpoK, a cytochrome P450 involved in biosynthesis of the anticancer agents epothilones A and B. Substrate-mediated rescue of a P450 enzyme. *Biochemistry*. 2004;43:14712–21.
44. Perera R, Sono M, Sigman JA, Pfister TD, Lu Y, Dawson JH. Neutral thiol as a proximal ligand to ferrous heme iron: implications for heme proteins that lose cysteine thiolate ligation on reduction. *Proc Natl Acad Sci USA*. 2003;100:3641–6.
45. Sun Y, Zeng W, Benabbas A, Ye X, Denisov I, Sligar SG, Du J, Dawson JH, Champion PM. Investigations of heme ligation and ligand switching in cytochromes p450 and p420. *Biochemistry*. 2013;52:5941–51.
46. Austin RN, Groves JT. Alkane-oxidizing metalloenzymes in the carbon cycle. *Metallomics*. 2011;3:775–87.
47. Noble MA, Miles CS, Chapman SK, Lysek DA, MacKay AC, Reid GA, Hanzlik RP, Munro AW. Roles of key active-site residues in flavocytochrome P450 BM3. *Biochem J*. 1999;339(Pt 2):371–9.
48. Lin Y, Lu P, Tang C, Mei Q, Sandig G, Rodrigues AD, Rushmore TH, Shou M. Substrate inhibition kinetics for cytochrome P450-catalyzed reactions. *Drug Metab Dispos*. 2001;29:368–74.
49. Chen B, Lee DY, Chang MW. Combinatorial metabolic engineering of *Saccharomyces cerevisiae* for terminal alkene production. *Metab Eng*. 2015;31:53–61.
50. Yang SJ, Rice KC, Brown RJ, Patton TG, Liou LE, Park YH, Bayles KW. A LysR-type regulator, CidR, is required for induction of the *Staphylococcus aureus* cidABC operon. *J Bacteriol*. 2005;187:5893–900.
51. McLaughlin JR, Murray CL, Rabinowitz JC. Unique features in the ribosome binding site sequence of the gram-positive *Staphylococcus aureus* b-lactamase gene. *J Biol Chem*. 1981;256:11283–91.
52. Munro AW, Lindsay JG, Coggins JR, Kelly SM, Price NC. Analysis of the structural stability of the multidomain enzyme flavocytochrome P-450 BM3. *Biochim Biophys Acta*. 1996;1296:127–37.
53. Manna SK, Mazumdar S. Reversible inactivation of cytochrome P450 by alkaline earth metal ions: auxiliary metal ion induced conformation change and formation of inactive P420 species in CYP101. *J Inorg Biochem*. 2008;102:1312–21.
54. Panicco P, Astuti Y, Fantuzzi A, Durrant JR, Gilardi G. P450 versus P420: correlation between cyclic voltammetry and visible absorption spectroscopy of the immobilized heme domain of cytochrome P450 BM3. *J Phys Chem B*. 2008;112:14063–8.
55. Hiner AN, Raven EL, Thorneley RN, Garcia-Canovas F, Rodriguez-Lopez JN. Mechanisms of compound I formation in heme peroxidases. *J Inorg Biochem*. 2002;91:27–34.

56. Lin JH, Lu AY. Role of pharmacokinetics and metabolism in drug discovery and development. *Pharmacol Rev.* 1997;49:403–49.
57. Korzekwa KR, Krishnamachary N, Shou M, Ogai A, Parise RA, Rettie AE, Gonzalez FJ, Tracy TS. Evaluation of atypical cytochrome P450 kinetics with two-substrate models: evidence that multiple substrates can simultaneously bind to cytochrome P450 active sites. *Biochemistry.* 1998;37:4137–47.
58. Shou M, Mei Q, Ettore MW Jr, Dai R, Baillie TA, Rushmore TH. Sigmoidal kinetic model for two co-operative substrate-binding sites in a cytochrome P450 3A4 active site: an example of the metabolism of diazepam and its derivatives. *Biochem J.* 1999;340(Pt 3):845–53.
59. Houston JB, Galetin A. Modelling atypical CYP3A4 kinetics: principles and pragmatism. *Arch Biochem Biophys.* 2005;433:351–60.
60. Ma L, Du L, Chen H, Sun Y, Huang S, Zheng X, Kim E-S, Li S. Reconstitution of the in vitro activity of the cyclosporine-specific P450 hydroxylase from *Sebekia benihana* and development of a heterologous whole-cell biotransformation system. *Appl Environ Microbiol.* 2015;81:6268–75.
61. Fujishiro T, Shoji O, Kawakami N, Watanabe T, Sugimoto H, Shiro Y, Watanabe Y. Chiral-substrate-assisted stereoselective epoxidation catalyzed by H₂O₂-dependent cytochrome P450_{SPa}. *Chem Asian J.* 2012;7:2286–93.
62. Onoda H, Shoji O, Watanabe Y. Acetate anion-triggered peroxygenation of non-native substrates by wild-type cytochrome P450s. *Dalton Trans.* 2015;44:15316–23.
63. Shoji O, Fujishiro T, Nakajima H, Kim M, Nagano S, Shiro Y, Watanabe Y. Hydrogen peroxide dependent monooxygenations by tricking the substrate recognition of cytochrome P450B5beta. *Angew Chem Int Ed Engl.* 2007;46:3656–9.
64. Ho SN, Hunt HD, Horton RM, Pullen JK, Pease LR. Site-directed mutagenesis by overlap extension using the polymerase chain reaction. *Gene.* 1989;77:51–9.
65. Wang ZJ, Peck NE, Renata H, Arnold FH. Cytochrome P450-catalyzed insertion of carbenoids into N–H bonds. *Chem Sci.* 2014;5:598–601.
66. Guengerich FP, Martin MV, Sohl CD, Cheng Q. Measurement of cytochrome P450 and NADPH-cytochrome P450 reductase. *Nat Protoc.* 2009;4:1245–51.
67. Berry EA, Trumpower BL. Simultaneous determination of hemes a, b, and c from pyridine hemochrome spectra. *Anal Biochem.* 1987;161:1–15.
68. Guan W, Zhao H, Lu X, Wang C, Yang M, Bai F. Quantitative analysis of fatty-acid-based biofuels produced by wild-type and genetically engineered cyanobacteria by gas chromatography-mass spectrometry. *J Chromatogr A.* 2011;1218:8289–93.

Submit your next manuscript to BioMed Central and we will help you at every step:

- We accept pre-submission inquiries
- Our selector tool helps you to find the most relevant journal
- We provide round the clock customer support
- Convenient online submission
- Thorough peer review
- Inclusion in PubMed and all major indexing services
- Maximum visibility for your research

Submit your manuscript at
www.biomedcentral.com/submit

